

DOI 10.24425/ae.2022.141684

Constrained optimization of the brushless DC motor using the salp swarm algorithm

ŁUKASZ KNYPÍŃSKI¹  , RAMESH DEVARAPALLI² , YVONNICK LE MENACH³ 

¹*Poznan University of Technology
Poland*

²*Department of EEE, Lendi Institute of Engineering and Technology
Vizianagaram, India*

³*Lille University, France*

e-mail:  lukasz.knypinski@put.poznan.pl, ramesh.ee@bitsindri.ac.in

(Received: 07.04.2022, revised: 19.05.2022)

Abstract: This paper presents an algorithm and optimization procedure for the optimization of the outer rotor structure of the brushless DC (BLDC) motor. The optimization software was developed in the Delphi Tiburón development environment. The optimization procedure is based on the salp swarm algorithm. The effectiveness of the developed optimization procedure was compared with genetic algorithm and particle swarm optimization algorithm. The mathematical model of the device includes the electromagnetic field equations taking into account the non-linearity of the ferromagnetic material, equations of external supply circuits and equations of mechanical motion. The external penalty function was introduced into the optimization algorithm to take into account the non-linear constraint function.

Key words: brushless DC motor, constrained optimization, finite element analysis, salp swarm algorithm

1. Introduction

Nowadays, heuristic algorithms [1] are commonly used in the process of constrained optimization of permanent magnet motors. Such optimization algorithms are well-suited to cooperation with mathematical models based on the finite element method (FEM) [2, 3]. Moreover, heuristic algorithms, often called metaheuristics are very effective to solve constrained optimization problems.



© 2022. The Author(s). This is an open-access article distributed under the terms of the Creative Commons Attribution-NonCommercial-NoDerivatives License (CC BY-NC-ND 4.0, <https://creativecommons.org/licenses/by-nc-nd/4.0/>), which permits use, distribution, and reproduction in any medium, provided that the Article is properly cited, the use is non-commercial, and no modifications or adaptations are made.

In the mathematical model describing electrical machines, it is necessary to take into account many coupled phenomena, such as: (a) electromagnetic field equations with the nonlinearity of the magnetic core, (b) Kirchhoff equations for electric circuits and (c) equations of the mechanical equilibrium equation [4–7]. The FEM models are very accurate, but also computationally time-consuming. Due to the long total time of the optimization process, highly convergent optimization algorithms are sought by researchers. In order to shorten the calculation time at the preliminary optimization stage, analytical models [8] or models with lumped parameters [9] are used.

In the present day, heuristic algorithms are developing rapidly. Among them, swarm intelligence algorithms form a very robust group. The following algorithms belong to this group: (a) the particle swarm optimization algorithm [10], (b) ant colony algorithm, (c) artificial bee colony, (d) firefly algorithm [11] and (e) salp swarm algorithm (SSA). The results of the latest research show a very good convergence of the SSA algorithm in comparison to other swarm intelligence methods [12].

The aim of this paper is to develop a constrained optimization procedure using the salp swarm algorithm. The convergence of the elaborated procedure was compared with the convergence of the genetic algorithm (GA) and particle swarm optimization (PSO). Next, the developed procedure was applied to optimize a brushless DC motor for an electric bike.

2. Salp swarm algorithm

Based on the swarming behaviour of salps, the salp swarm algorithm was proposed in 2017 by Mirjalili [13]. The way in which salps move is similar to jellyfish and their living environments are very difficult to access, usually on the ocean floor [14]. The nature of the swarm formation known as the salp chain was mathematically modelled by treating a group of salps as a leader and its followers. The name itself defines that the follower salps will follow the leader salp in the salp chain. The behaviour of the leader salp's positioning within the search space can be mathematically modelled in the form of Eq. (1)

$$\mathbf{x}^l = \begin{cases} \mathbf{x}^s + a_1 [a_2 (\mathbf{x}_{\max} - \mathbf{x}_{\min}) + \mathbf{x}_{\min}] & \text{for } a_3 \geq 0 \\ \mathbf{x}^s - a_1 [a_2 (\mathbf{x}_{\max} - \mathbf{x}_{\min}) + \mathbf{x}_{\min}] & \text{for } a_3 < 0 \end{cases}, \quad (1)$$

where: \mathbf{x} is the vector composed of the design variable of the optimization procedure, \mathbf{x}^l is the position of the leader, \mathbf{x}^s is the target foodstuff, a_1 , a_2 , and a_3 are the arbitrary values, \mathbf{x}_{\min} and \mathbf{x}_{\max} are the lower and upper limits of vectors for each design variable.

The positions of the leaders and followers are determined by using the following equation:

$$\mathbf{x}^f = \frac{1}{2} \alpha \tau^2 + \beta \tau f \geq 2. \quad (2)$$

Equation (2) is derived from Newton's law of motion with the time τ , and initial speed β_0 [15].

The salp swarm coefficient a_1 for each k^{th} iteration is determined by Eq. (3)

$$a_1 = 2e^{-\left(\frac{k}{k_{\max}}\right)}, \quad (3)$$

where k_{\max} is the maximum number of iteration.

The balance between the exploration and exploitation phases can be achieved by proper selection of the a_1 factor. It is obtained for a particular iteration k from Eq. (3) at the total number of iterations k_{\max} . In addition, arbitrary values a_2 , and a_3 are selected randomly in the range $[0, 1]$.

The flow chart of the SSA is presented in Fig. 1.

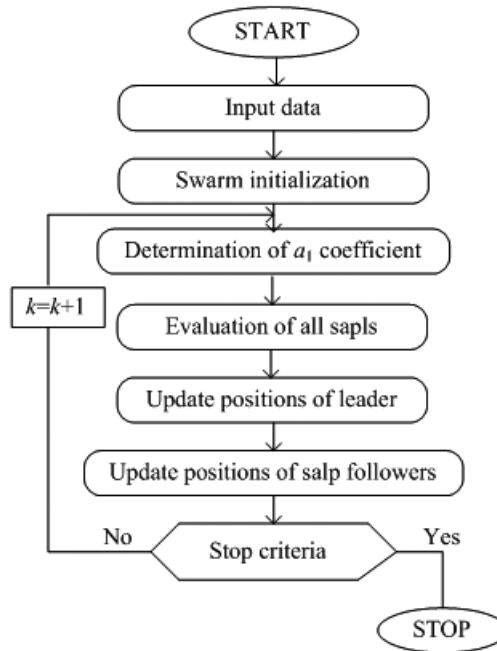


Fig. 1. Flowchart of the salp swarm algorithm

3. Test of the algorithm by the using the benchmark functions

The developed optimization procedure for the optimal synthesis of a BLDC motor was tested using the benchmark functions. Each heuristic algorithm is a stochastic algorithm [16]. The quality of the optimal solution can depend on: the starting population and the random numbers used to determine the new positions of the salps. In order to verify the correctness of the algorithm, the global minimum point of the Goldstein–Price function $f_1(x_1, x_2)$ was searched [17]. The f_1 function described by Formula (4) is

$$f_1(x_1, x_2) = \left[1 + (x_1 + x_2 + 1)^2 \left(19 - 14x_1 + 3x_1^2 - 14x_2 + 6x_1x_2 + 3x_2^2 \right) \right] \cdot \left[30 + (2x_1 - 3x_2)^2 \left(18 - 32x_1 + 12x_1^2 + 48x_2 - 36x_1x_2 + 27x_2^2 \right) \right], \quad (4)$$

where: x_1 is in the range $(-3.0, 3.0)$, x_2 is in the range $(-3.0, 3.0)$.

The analyzed function has one global minimum [18] at the point $(0, -1)$, and $f_1(0, -1)$ is equal to 3. Additionally, the Goldstein–Price function has three local minima points: (a) $(1.2, 0.8)$, (b) $(1.8, 0.2)$ and (c) $(-0.6, -0.4)$. The plot of the Goldstein–Price function is presented in Fig. 2.

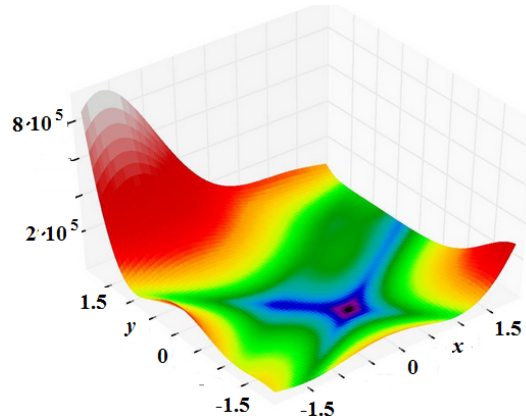


Fig. 2. Visualization of the Goldstein–Price function

Next, the calculation was performed for the six-hump camel function f_2 . The f_2 function is defined by Eq. (5)

$$f_2(x_1, x_2) = x_1^2 \left(4 - 2.1x_1^2 + \frac{x_1^4}{3} \right) + x_1x_2 + x_2^2 (4x_2^2 - 4), \quad (5)$$

where: x_1 is in the range $(-3.0, 3.0)$, x_2 is in the range $(-3.0, 3.0)$.

The multimodal six-hump camel function has two global minima. Both global minima are equal to -1.0316 and have coordinates $(0.0899, -0.7126)$ or $(-0.0899, 0.7126)$.

In the case of heuristic algorithms, the solutions obtained may depend on many coefficients. In order to obtain more reliable results, the optimization process was run 20 times for random positions of the salps during the initialization procedure.

The computations were done by the following parameters of the SSA: the number of salps, $N = 50$, and the maximum number of iterations, $k_{\max} = 80$. The statistical analysis has been performed. The average, best, worst and standard deviation (SD) results of the optimization process were calculated.

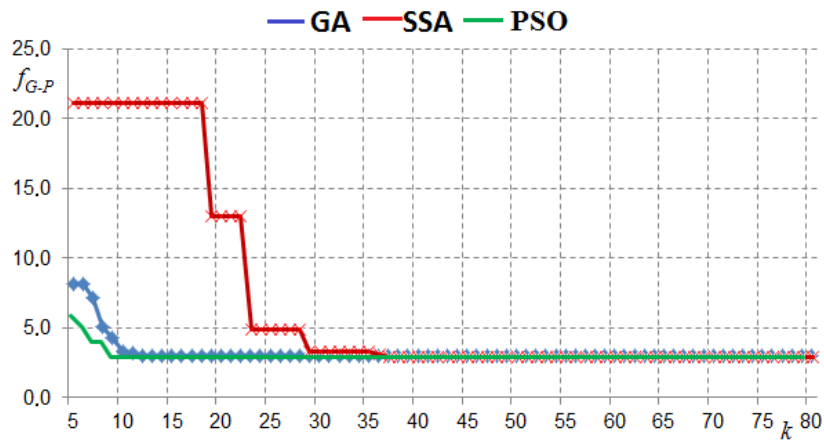
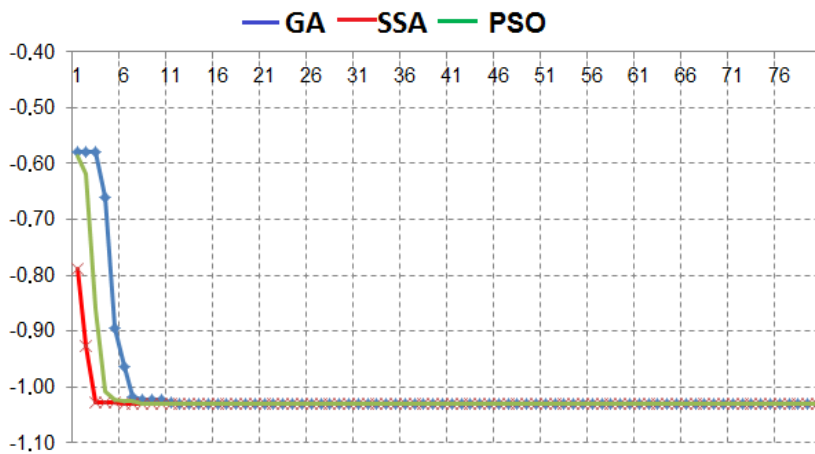
Next, the simulation calculations were executed for the GA and PSO [15]. The number of individuals was 50. The probability of mutation was $p_m = 0.005$. The values of the constant factors for PSO algorithm were used: $w = 0.2$, $c_1 = 0.35$ and $c_2 = 0.45$. The results of the computations are presented in Table 1.

When comparing the computer simulations for both benchmark functions, it can be observed that the best results are similar for all analyzed optimization algorithms. Better values of the average function and standard deviations were obtained for the SSA.

Convergence curves for the best optimization process for the SSA, GA and PSO are shown in Fig. 3 and Fig. 4.

Table 1. Statistical analysis to benchmark functions for compared optimization algorithms

Algorithm	Benchmark function	Range	Best	Worst	Average	SD
SSA	f_1	(-3.5, 3.5)	3.000000	3.000001	3.0000001	0.0000001
	f_2	(-3.0, 3.0)	-1.031628	-1.031627	-1.031628	0.0000025
GA	f_1	(-3.5, 3.5)	3.000011	3.000248	3.000264	0.0006112
	f_2	(-3.0, 3.0)	-1.031628	-1.026659	-1.031345	0.0011091
PSO	f_1	(-3.5, 3.5)	3.000001	3.000034	3.000026	0.0000456
	f_2	(-3.0, 3.0)	-1.031628	-1.00955	-1,029354	0.0036027

Fig. 3. The comparison of convergence curves for f_1 Fig. 4. The comparison of convergence curves for f_2

It can be observed, that the SSA allows one to obtain better results than the GA. The genetic algorithm has faster convergence than the SSA. The convergence curve of the PSO is very fast for the f_1 benchmark function. It can be observed, that after ten iterations of the algorithm the position of the leader is near the global minimum.

The SSA belongs to swarm intelligence algorithms. During the process of searching for a global extreme, all individuals cooperate with each other. The process of searching for the global minimum of the “heart” benchmark function is shown in Fig. 5. The red point denotes the global minimum of the analyzed function.

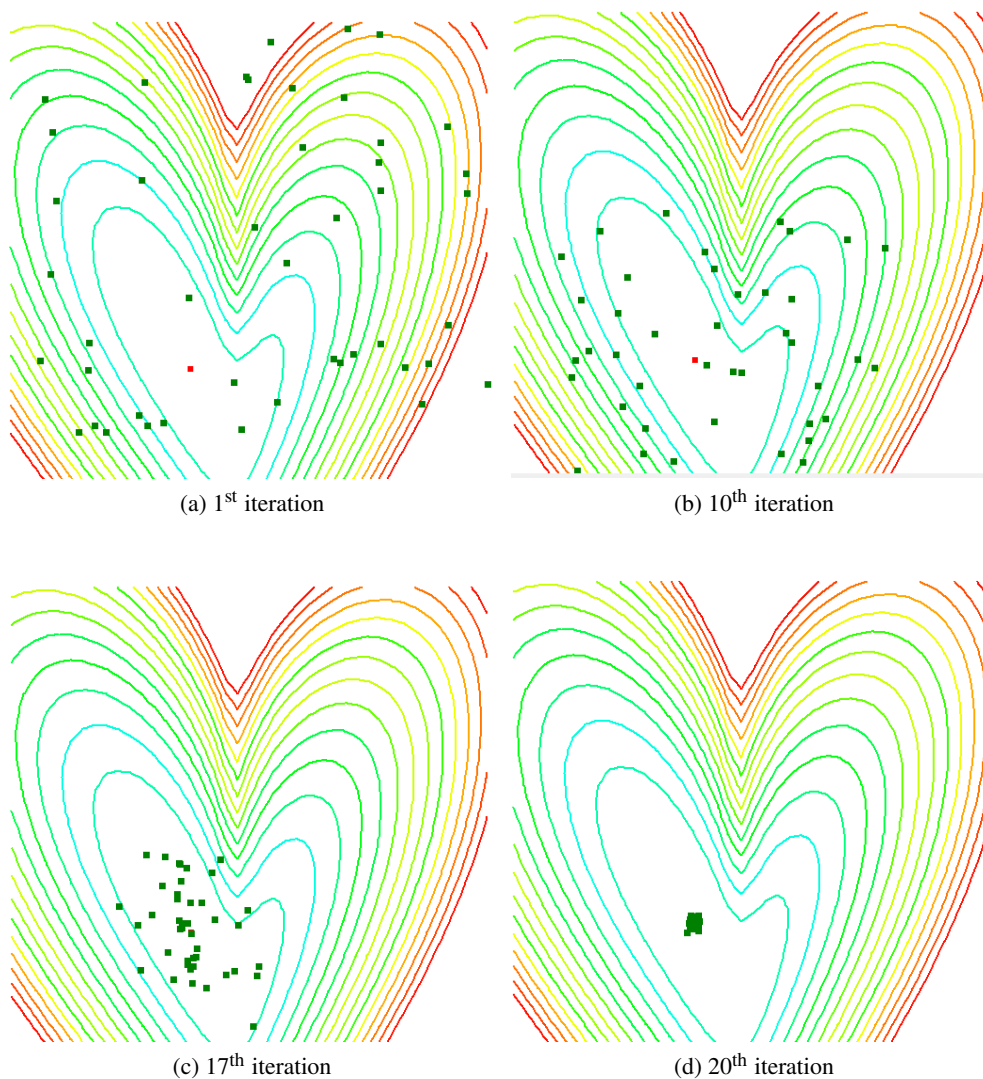


Fig. 5. Distribution of the slaps in selected iterations

Based on the distribution of individuals, it can be concluded that salps search the permissible area for up to 10 iterations. Subsequent iterations show swarming behavior when all salps are gathered around the extreme point. In the SSA, the particles concentrate slower around the global minimum point than in the PSO, in which the swarming behavior is very fast.

4. Field-circuit model of BLDC

In permanent magnet machines, the electromagnetic field is excited simultaneously by permanent magnets and stator windings. The equations describing the electromagnetic field in devices containing soft ferromagnetic material, permanent magnets and areas with constant magnetic permeability, are [19]:

$$\operatorname{curl} \left(\frac{1}{\mu} \operatorname{curl} \mathbf{A} \right) = \mathbf{J}_u + \mathbf{J}_M, \quad (6)$$

$$\mathbf{J}_u = \sigma \left(\operatorname{grad} V_e - \frac{\partial \mathbf{A}}{\partial t} \right), \quad (7)$$

where: μ is the magnetic permeability, \mathbf{A} is the magnetic vector potential, \mathbf{J}_u is the vector of current density in the stator winding, \mathbf{J}_M is the vector of magnetizing current density in the regions with permanent magnets, σ is the electric conductivity, V_e is the scalar electric potential.

In the regions containing permanent magnets, the magnetizing current density vector depends on the magnetization vector \mathbf{M} .

$$\mathbf{J}_M = \operatorname{curl} \mathbf{M}, \quad (8)$$

where \mathbf{M} is the magnetization vector within the permanent magnet area.

The electric machines are usually supplied by voltage sources. Due to the non-linearity of the ferromagnetic core and back-electromotive force induced in the stator winding, the waveforms of current waveforms in the phases of the BLDC motor are not known in advance. These waveforms are necessary to determine the electromagnetic field distribution. Thus, it is necessary to take into consideration the Kirchhoff equations for electric circuits

$$\frac{d\boldsymbol{\Psi}}{dt} + \mathbf{R}\mathbf{i} = \mathbf{u}, \quad (9)$$

where: \mathbf{u} is the vector of supply voltages, $\boldsymbol{\Psi}$ is the matrix of flux linkage, \mathbf{R} is the diagonal matrix of winding resistances, \mathbf{i} is the vector composed from phase currents.

In transient states (start-up and load change), the rotational velocity is not known in advance. Therefore, it is necessary to take into account the mechanical equilibrium equation

$$J_i \frac{d\omega}{dt} = T - T_l - B\omega, \quad (10)$$

where: J_i is the moment of inertia, ω is the angular velocity, T is the electromagnetic torque, T_l is the loading torque, B is the friction constant.

A two-dimensional (2-D) finite element method (FEM) model of the BLDC motor was developed. In order to solve the non-linear system of FEM equations the iterative Newton-Raphson process was adopted. The set of coupled field-circuit equations can be written in the

form [20]

$$\begin{bmatrix} \mathbf{H}_n^k & -\mathbf{z} \\ \mathbf{z}^T & \Delta t \mathbf{R} \end{bmatrix} \begin{bmatrix} \delta \Phi_n^k \\ \delta \mathbf{i}_n^k \end{bmatrix} = \begin{bmatrix} \Theta_{Mn} - \mathbf{S}_n^k \Phi_n^{k-1} + \mathbf{z} \mathbf{i}_n^{k-1} \\ \Delta t \mathbf{u}_n + \mathbf{z}^T \Phi_{n-1} - \mathbf{z}^T \Phi_n^{k-1} - \Delta t \mathbf{R} \mathbf{i}_n^{k-1} \end{bmatrix}, \quad (11)$$

where: \mathbf{H}_n^k is the Hessian matrix of the Newton–Raphson process, \mathbf{z} is the matrix of turn numbers associated with the nodes within the windings area, $\Delta t = t_n - t_{n1}$ is the time step length, Θ_{Mn} is the vector of magneto-motive forces in the permanent magnets area, \mathbf{S}_n is the stiffness matrix at the time t_n , $\Phi_n = l \mathbf{A}_n$ is the vector of nodal potentials multiplied by the machine length l , k is the Newton–Raphson iteration, $\delta \Phi_n^k = \Phi_n^k - \Phi_n^{k-1}$ and $\delta \mathbf{i}_n^k = \mathbf{i}_n^k - \mathbf{i}_n^{k-1}$ are the unknown vectors Φ_n^k and \mathbf{i}_n^k increments.

All parameters (T_{av} and ε) used in the optimization procedure were calculated on the basis of the electromagnetic field distribution.

The pulsation factor is determined

$$\varepsilon = \frac{T_{max} - T_{min}}{T_{av}} 100\%, \quad (12)$$

where: T_{max} , T_{min} are the maximum and minimum electromagnetic torque values, T_{av} is the average electromagnetic torque.

5. Optimization of BLDC motor

To analyze the convergence of the salp swarm algorithm, the optimization of the outer rotor BLDC motor was executed. The structure of the BLDC motor was described by four design variables: $s_1 = \delta$ – air gap length, $s_2 = h_{PM}$ – the height of the permanent magnet, $s_3 = \tau_{PM}$ – a span of the permanent magnet, $s_4 = h_{FE} = \xi h_{PM}$ – the height of the ferromagnetic tooth. The structure of the BLDC motor is presented in Fig. 6.

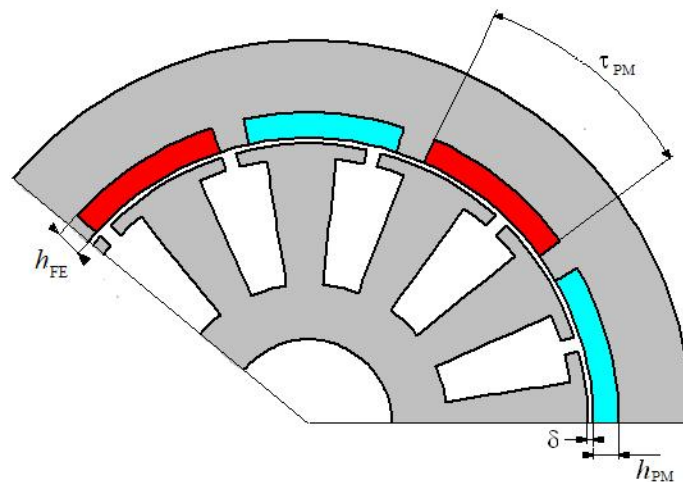


Fig. 6. Structure of BLDC motor

The more important steady-state parameters in BLDC motors are: (a) average torque and (b) pulsation factor. The electromagnetic torque is very frequently maximized while the pulsation factor is minimized [21–23].

The adopted objective function for the i^{th} salp has the following form:

$$f^i(\delta, h_{\text{PM}}, \tau_{\text{PM}}, h_{\text{FE}}) = \frac{T_{\text{av}}^i(\delta, h_{\text{PM}}, \tau_{\text{PM}}, h_{\text{FE}})}{T_{\text{av}0}}, \quad (13)$$

where: $T_{\text{av}}^i(\delta, h_{\text{PM}}, \tau_{\text{PM}}, h_{\text{FE}})$ is the average value of electromagnetic torque for the i -th salp and $T_{\text{av}0}$ is the average value of electromagnetic torque after the initiation procedure.

The non-linear constraint function is taken into account. During the optimization process, the permissible pulsation factor was imposed [24]. The constraint function was normalized and had the following form:

$$g^i(\delta, h_{\text{PM}}, \tau_{\text{PM}}, h_{\text{FE}}) = \frac{\varepsilon^i(\delta, h_{\text{PM}}, \tau_{\text{PM}}, h_{\text{FE}}) - \varepsilon_{\chi}}{\varepsilon} \leq 0, \quad (14)$$

where ε_{χ} was the permissible pulsation factor.

The SSA convergence is not fast at the beginning of the optimization process (see Fig. 3), therefore an external penalty can be effective. In the approach with an external penalty, a modified objective function h is created.

$$h_m^i(\delta, h_{\text{PM}}, \tau_{\text{PM}}, h_{\text{FE}}) = \begin{cases} f^i & \text{for } \varepsilon^i \leq \varepsilon_{\chi} \\ f^i - P^i & \text{for } \varepsilon^i > \varepsilon_{\chi} \end{cases}, \quad (15)$$

where: m is the number of external penalty iterations, P is the penalty component.

In the external penalty function, the penalty component represents the penalty for exceeding the permissible value of the pulsation factor ε_{χ} . The value of P depends on the number (m) of external penalty iterations and is formed as follows:

$$P_m^i(\delta, h_{\text{PM}}, \tau_{\text{PM}}, h_{\text{FE}}) = r^m g^i(\delta, h_{\text{PM}}, \tau_{\text{PM}}, h_{\text{FE}}), \quad (16)$$

where r is the penalty coefficient [10].

Optimization calculations were performed for the following parameters: the number of salps is equal to 45, the maximum number of iterations is equal to 40, the permissible pulsation factor $\varepsilon_{\chi} \leq 0.15$ and penalty coefficient $r = 1.2$. The calculation was performed for m equal to 4 (i.e. the number of iterations of the slap swarm algorithm executed in one external penalty iteration). The course of the optimization process for the best individual is presented in Table 2.

According to the results shown in Table 2, the optimal results were obtained after about 20 iterations of the SSA. In earlier iterations of the optimization process, a successive increase in the average value of the electromagnetic torque and a decrease in the value of the pulsation coefficient can be observed.

Next, the distribution of the salps in the selected iterations of the optimization process of the BLDC motor in the space δ and h_{PM} are presented in Fig. 7.

Based on the distributions of the salps in the space of two design variables, it can be observed that until the 10th iteration, the salps recognize the area around the best-adapted individual. In the 10th iteration, most of the slaps have a value of δ in the range of 1.25, 1.32 mm.

Table 2. Comparison of the results for selected iterations of optimization process

k	δ	h_{PM}	τ_{PM}	ξ	T_{av}	ε	h
1	1.256	4.152	0.751	0.89	2.645	0.371	0.3435
5	1.249	4.713	0.751	0.84	2.693	0.268	0.3657
9	1.305	4.956	0.751	0.82	2.751	0.213	0.4102
13	1.312	4.984	0.833	0.81	2.749	0.193	0.7765
16	1.315	4.987	0.833	0.81	2.751	0.189	0.9365
20	1.153	4.348	0.917	0.80	2.756	0.151	1.2172
40	1.153	4.348	0.917	0.80	2.786	0.151	1.2172

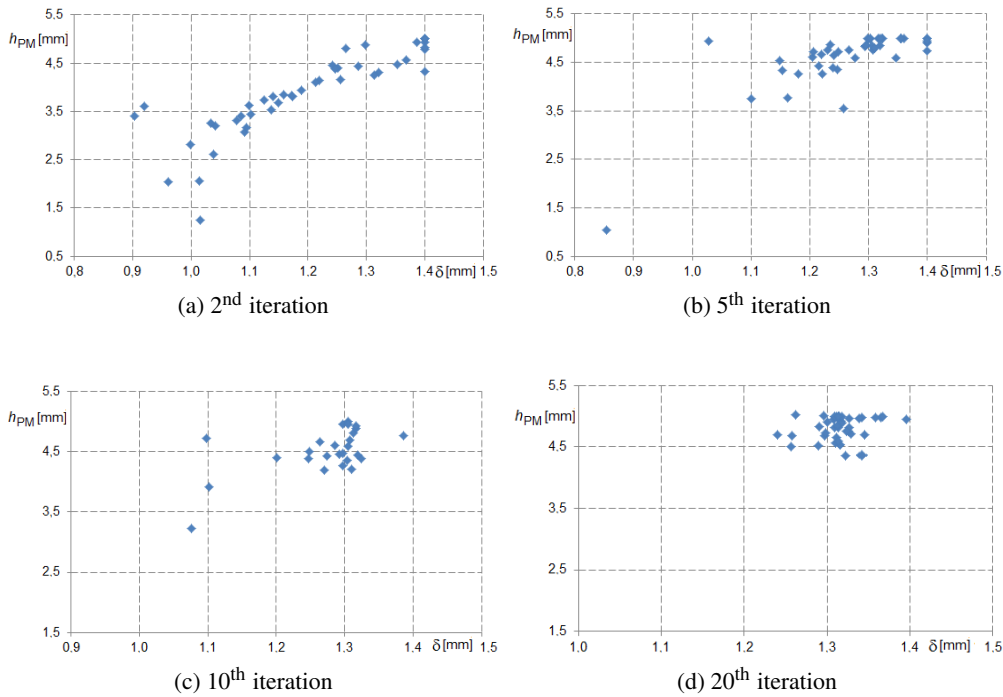


Fig. 7. Distribution of the slaps in selected iterations

Next, the FEM calculations for optimal values of design variables at: (a) the 1st iteration and (b) the last iteration optimization process were executed. The obtained waveforms of electromagnetic torque are presented in Fig. 8.

It can be observed that for the best salp in the 1st iteration, the maximum value of electromagnetic torque is greater than the maximum value of torque for the best salp in the last iteration.

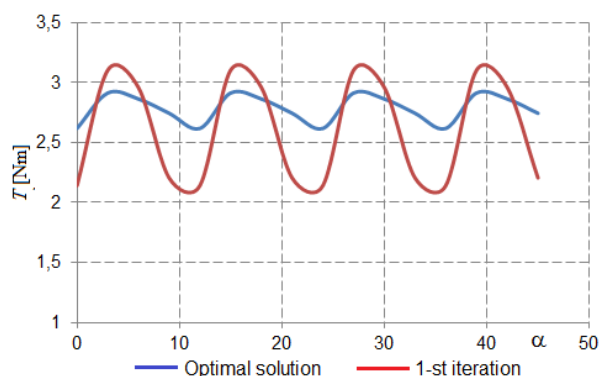


Fig. 8. The waveforms of electromagnetic torque for selected iterations of optimization process

Despite the bigger value of the maximum value of the electromagnetic torque, the mean value of the output torque is lower in the first iteration. The reduction of the pulsation coefficient by approximately 59% was obtained during the optimization process.

6. Conclusions

This paper presents the application of the salp swarm algorithm for constrained optimization of the BLDC motor. The salp swarm algorithm belongs to swarm intelligence optimization algorithms. The developed optimization procedure was tested on the analytical functions. Next, the optimization procedure was tied with an FEM model describing coupled phenomena in the BLDC motor. The result of the optimization process for the BLDC motor confirmed the effectiveness of the SSA in solving constrained optimization tasks.

The performed research has shown, that the SSA is a very interesting alternative to the classical particle swarm algorithm. The process of searching for the global extreme for the SSA is slightly slower in relation to the PSO. Therefore, in the case of connecting the SSA with the external penalty method, the external iteration linked with the increasing penalty component may be changed more slowly than in the PSO algorithm. The obtained results encourage a deeper analysis of such an algorithm.

Acknowledgements

This research was funded by the Polish Government, grant number [0212/SBAD/00572].

References

- [1] Seong Oh B., Cho J., Choi B., Wone Choi H., Soo Kim M., Lee G., *Application of Heuristic Algorithms for Design Optimization of Industrial Heat Pump*, International Journal of Refrigeration, vol. 134, pp. 1–15 (2022), DOI: [10.1016/j.ijrefrig.2021.11.002](https://doi.org/10.1016/j.ijrefrig.2021.11.002).

- [2] Mutluer M., Sahman A., Cunkas M., *Heuristic optimization based on penalty approach for surface permanent magnet synchronous machines*, Arabian Journal for Science and Engineering, vol. 45, pp. 6751–6767 (2020), DOI: [10.1007/s13369-020-04689-y](https://doi.org/10.1007/s13369-020-04689-y).
- [3] Knypiński Ł., Pawełkoszek K., Le Menach Y., *Optimization of low-power line-start PM motor using gray wolf metaheuristic algorithm*, Energies, vol. 13, no. 1186 (2020), DOI: [10.3390/en13051186](https://doi.org/10.3390/en13051186).
- [4] Barański M., Szelaż W., Łyskawiński W., *Experimental and Simulation Studies of Partial Demagnetization Process of Permanent Magnets in Electric Motors*, IEEE Transactions on Energy Conversion, vol. 36, no. 4, pp. 3137–3145 (2021), DOI: [10.1109/TEC.2021.3082903](https://doi.org/10.1109/TEC.2021.3082903).
- [5] Pettes-Duler M., Roboam X., Sareni B., Lefevre Y., Llibre J.F., Fénot M., *Multidisciplinary Design Optimization of the Actuation System of a Hybrid Electric Aircraft Powertrain*, Electronics, vol. 10, no. 1297 (2021), DOI: [10.3390/electronics10111297](https://doi.org/10.3390/electronics10111297).
- [6] Marault J., Tounzi A., Gillon F., Hecquet M., *Use of current sheet coupled to an analytical tool to analyze by FEM the harmonic content of armature winding distribution*, COMPEL, vol. 39, no. 6, pp. 1329–1344 (2020), DOI: [10.1108/COMPEL-01-2020-0052](https://doi.org/10.1108/COMPEL-01-2020-0052).
- [7] Wardach M., Paplicki P., Palka R., *A Hybrid Excited Machine with Flux Barriers and Magnetic Bridges*, Energies, vol. 11, no. 676, pp. 1–8 (2018), DOI: [10.3390/en11030676](https://doi.org/10.3390/en11030676).
- [8] Fleuret E., Franck Scuiller F., Jean-Frédéric Charpentier J.F., *Analytical Models for Fast and Accurate Calculation of Electromagnetic Performances of Segmented Permanent Magnet Synchronous Machines with Large Angular Gap*, Applied Sciences, vol. 11, no. 459, pp. 1–9 (2021), DOI: [10.3390/app11010459](https://doi.org/10.3390/app11010459).
- [9] Ullah W., Khan F., Umair M., *Lumped parameter magnetic equivalent circuit model for design of segmented PM consequent pole flux switching machine*, Engineering Computations, vol. 38, no. 2, pp. 572–585 (2021), DOI: [10.1108/EC-04-2020-0201](https://doi.org/10.1108/EC-04-2020-0201).
- [10] Knypiński Ł., *Constrained optimization of line-start PM motor based on the gray wolf optimizer*, Eksploatacja i Niezawodność – Maintenance nad Reliability, vol. 23, no. 1, pp. 1–10 (2021), DOI: [10.17531/ein.2021.1.1](https://doi.org/10.17531/ein.2021.1.1).
- [11] Arsyad H., Suyuti A., Mawar Said S., Syam Akil Y., *Multi-objective dynamic economic dispatch using Fruit Fly Optimization method*, Archives of Electrical Engineering, vol. 70, no 2, pp. 351–366 (2021), DOI: [10.24425/aee.2021.136989](https://doi.org/10.24425/aee.2021.136989).
- [12] Wang S., Jia H., Peng X., *Modified salp swarm algorithm based multilevel thresholding for color image segmentation*, Mathematical Biosciences and Engineering, vol. 17, no. 1, pp. 700–724 (2020), DOI: [10.3934/mbe.2020036](https://doi.org/10.3934/mbe.2020036).
- [13] Mirjalili S., Gandomi A.H., Zahra Mirjalili S., Saremi S., Faris H., Mohammad Mirjalili S., *Salp Swarm Algorithm: A bio-inspired optimizer for engineering design problems*, Advances in Engineering Software, vol. 114, pp. 163–191 (2017), DOI: [10.1016/j.advengsoft.2017.07.002](https://doi.org/10.1016/j.advengsoft.2017.07.002).
- [14] Madina L.P., Kremerb P., Wiebea P.H., Purcellc J.E., Horgana E.H., Nemażiec D.A., *Periodic swarms of the salp Salpa aspera in the Slope Water off the NE United States: Biovolume, vertical migration, grazing, and vertical flux*, Deep Sea Research Part I: Oceanographic, vol. 53, no 5, pp. 804–819 (2006), DOI: [10.1016/j.dsr.2005.12.018](https://doi.org/10.1016/j.dsr.2005.12.018).
- [15] Mahmood M.A., Al-Anbarri K.A., *Optimum unit commitment solution of a power system based on slap swarm algorithm*, Journal of Engineering and Sustainable Development, pp. 1–13 (2021), DOI: [10.31272/jeasd.conf.2.1.12](https://doi.org/10.31272/jeasd.conf.2.1.12).
- [16] Devarapalli R., Bhattacharyya B., Sinha N.K., *An intelligent EGWO-SCA-CS algorithm for PSS parameter tuning under system uncertainties*, International Journal of Intelligent Systems, vol. 35, no. 10, pp. 1520–1569 (2020), DOI: [10.1002/int.22263](https://doi.org/10.1002/int.22263).

- [17] Knypiński Ł., *Performance analysis of selected metaheuristic optimization algorithms applied in the solution of an unconstrained task*, COMPEL (2022), DOI: [10.1108/COMPEL-07-2021-0254](https://doi.org/10.1108/COMPEL-07-2021-0254).
- [18] <https://www.sfu.ca/~ssurjano/goldpr.html>, accessed January 2022.
- [19] Jędrzycka C., Sujka P., Szeląg W., *The influence magnetic hysteresis on magnetorheological fluid clutch operation*, COMPEL, vol. 28, no. 3, pp. 711–721 (2009), DOI: [10.1108/03321640910940963](https://doi.org/10.1108/03321640910940963).
- [20] Knypiński Ł., Nowak L., *Fidel-circuit simulation of the dynamics of the outer rotor permanent magnet brushless DC motor*, COMPEL, vol. 30, no. 2, pp. 929–440 (2011), DOI: [10.1108/03321641111110898](https://doi.org/10.1108/03321641111110898).
- [21] Pourjafari M., Fallah Choolabi E., Jafar Bolan M., *Optimum Design of BrushLess DC Motor with Minimum Torque Pulsation using FEM and PSO*, Amirkabir International Journal of Electrical and Electronics Engineering, vol. 44, no. 2, pp. 59–70 (2012), DOI: [10.22060/ej.2012.360](https://doi.org/10.22060/ej.2012.360).
- [22] Knypiński Ł., Kuroczycki S., Marquez F.P.G., *Minimization of Torque Ripple in the Brushless DC Motor Using Constrained Cuckoo Search Algorithm*, Electronics, vol. 10, no. 18, pp. 2299–1–2299–20 (2021), DOI: [10.3390/electronics10182299](https://doi.org/10.3390/electronics10182299).
- [23] Ge J., Xu W., Liu Y., Xiong F., *Novel Equivalent Circuit Model Applicable to All Operation Modes for Brushless Doubly-Fed Induction Machines*, IEEE Transactions on Industrial Electronics (2022), DOI: [10.1109/TIE.2022.3144567](https://doi.org/10.1109/TIE.2022.3144567).
- [24] De Gregoriis D., Naets F., Kindt P., *Application of a-priori hyper-reduction to the nonlinear dynamic finite element simulation of a rolling car tire*, Journal of Computational and Nonlinear Dynamics, vol. 14; no. 11, pp. 111009–1–111009–13 (2019), DOI: [10.1115/1.4043892](https://doi.org/10.1115/1.4043892).